This is a repository copy of *Spin-Crossover and the LIESST Effect in [FexCo1–x(bpp)2] [BF4]2 (1.00 ≤ x ≤ 0.77). Comparison with Bifunctional Solid Solutions of Iron and Cobalt Spin-Crossover Centers*.

White Rose Research Online URL for this paper:
http://eprints.whiterose.ac.uk/111499/

Version: Accepted Version

Accepted Manuscript

Spin-Crossover and the LIESST Effect in [Fe $_x$ Co$_{1-}$ $_x$(bpp)$_2$][BF$_4$]$_2$ (1.00 x 0.77). Comparison with Bifunctional Solid Solutions of Iron and Cobalt Spin-Crossover Centers

Malcolm A. Halcrow, Guillaume Chastanet

Spin-Crossover and the LIESST Effect in [Fe$_x$Co$_{1−x}$(bpp)$_2$][BF$_4$]$_2$ (1.00 ≤ x ≤ 0.77). Comparison with Bifunctional Solid Solutions of Iron and Cobalt Spin-Crossover Centers

Malcolm A. Halcrow [1],* and Guillaume Chastanet [2],*

[1] School of Chemistry, University of Leeds, Woodhouse Lane, Leeds LS2 9JT, UK; E-Mail: m.a.halcrow@leeds.ac.uk

[2] CNRS, University of Bordeaux, ICMCB, UPR 9048, F-33600 Pessac, France; E-Mail: chastanet@icmcb-bordeaux.cnrs.fr

TOC Entry
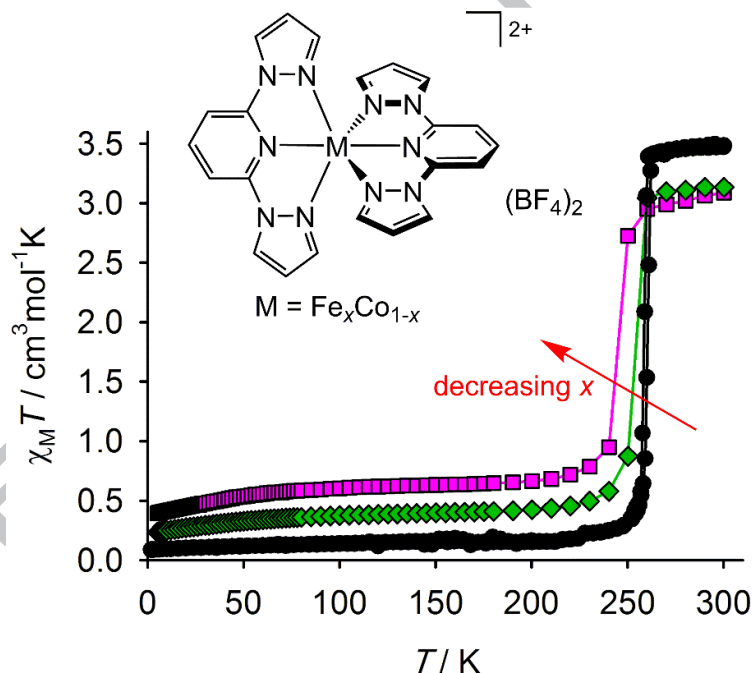
Thermal spin-crossover in [Fe$_x$Co$_{1−x}$(bpp)$_2$][BF$_4$]$_2$ (bpp = 2,6-di{pyrazol-1-yl}pyridine; 1.00 ≤ x ≤ 0.77) only involves the iron centers, and increasing the cobalt dopant concentration leads to a reduction in $T_{1/2}$ and a loss of cooperativity. The materials exhibit the LIESST effect, with all three samples presenting the same T(LIESST) value. LIESST relaxation kinetics have a clear multistep character, which has not been detected before in samples derived from [Fe(bpp)$_2$][BF$_4$]$_2$.

Abstract: Co-crystallization of $[Fe(bpp)_2][BF_4]_2$ and $[Co(bpp)_2][BF_4]_2$ (bpp = 2,6-di{pyrazol-1-yl}pyridine) from nitromethane-diethyl ether yields homogeneous polycrystalline materials analysing as $[Fe_xCo_{1-x}(bpp)_2][BF_4]_2$ ($1.00 \leq x \leq 0.77$). Thermal spin-crossover in these materials only involves the iron centers, and increasing the cobalt dopant concentration leads to a reduction in $T_{\frac{1}{2}}$ and a loss of cooperativity. The materials exhibit the LIESST effect, with all three samples presenting the same T(LIESST) value. LIESST relaxation kinetics have a clear multistep character, which has not been detected before in samples derived from $[Fe(bpp)_2][BF_4]_2$. Magnetic susceptibility and low-temperature crystallographic data are also presented for the pure precursor complex $[Co(bpp)_2][BF_4]_2$.

Keywords: iron; cobalt; N-donor ligand; spin-crossover; magnetic measurements

1. Introduction

Spin-crossover compounds continue to be heavily studied [1-3], 50 years after the phenomenon was first identified [4], because of their utility as switching centers in nanoscience [5], molecular devices [6, 7] and other types of functional material [8, 9]. A particular goal of spin-crossover researchers is to produce multifunctional compounds, that use spin-crossover switching to modulate another property of a material [10]. For example, materials showing fluorescence [11-15], resistivity [16-20] and dielectric [21-24] that responds to their thermal spin-transition are now well-established.

Six years ago we introduced a new approach towards this goal by doping functional complex cations into a spin-crossover host lattice [25-29]. The method exploits the fact that spin-crossover complexes of the $[Fe(bpp)_2]X_2$ type (bpp = 2,6-di{pyrazol-1-yl}pyridine; X = BF_4^- or ClO_4^-) often adopt the "terpyridine embrace" crystal packing [30], which is also exhibited by functional complexes of other tris-heterocyclic ligands such as $[M(terpy)_2]^{2+}$ (terpy = 2,2':6',2''-terpyridine) [31]. Although they are not perfectly isostructural as pure compounds, $[Fe(bpp)_2]X_2$ and $[M(terpy)_2]X_2$ complex salts co-crystallize into homogeneous $[Fe(bpp)_2]_y[M(terpy)_2]_{1-y}[BF_4]_2$ solid solutions, which are single-phase materials when y is not close to 0.5. In this way, we have obtained $[Fe(bpp)_2]_y[M(terpy)_2]_{1-y}[BF_4]_2$ materials that show both spin-crossover and fluorescence (M = Ru) [25, 26], or exhibit allosteric switching of two different spin-crossover centers in the same material (M = Co) [26, 27].

$[M(bpp)_2]^{2+}$
M = Fe or Co
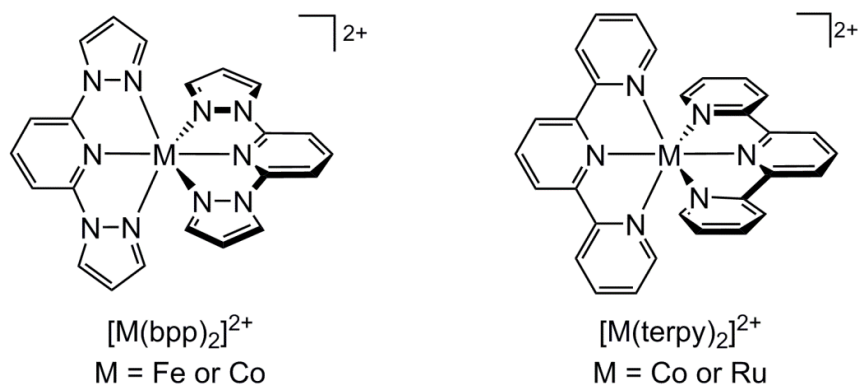
$[M(terpy)_2]^{2+}$
M = Co or Ru

Scheme 1. The complexes referred to in this paper.

The latter result, of simultaneous spin-crossover in the iron host-lattice and cobalt dopant in $[Fe(bpp)_2]_y[Co(terpy)_2]_{1-y}[BF_4]_2$, is particularly noteworthy. It is probably caused by the 2 % volume change of the $[Fe(bpp)_2][BF_4]_2$ host lattice during the high→low spin-transition [32]. The resultant change in lattice pressure on the $[Co(terpy)_2]^{2+}$ dopant induces it to change its own spin state in sympathy [33]. Notably, this allosteric behavior is observed during spin-state switching under both thermodynamic (thermal) and kinetic (LIESST effect [34]) conditions [26]. This is the only known example of LIESST behavior in a cobalt complex. More generally, this result could be expanded into a more general method to induce new functionality in inert molecules, by doping them into a switchable host lattice. As a first investigation of the generality of our result, we report here a new series of iron/cobalt solid solutions, $[Fe_xCo_{1-x}(bpp)_2][BF_4]_2$. While these are isostructural with our $[Fe(bpp)_2]_y[Co(terpy)_2]_{1-y}[BF_4]_2$ materials, the new compounds differ in that their iron and cobalt centers are supported by the same bpp ligand.

2. Results and Discussion
2.1 Characterization of the precursor compounds

The bpp ligand [35], and the precursor complexes $[Fe(bpp)_2][BF_4]_2$ [32] and $[Co(bpp)_2][BF_4]_2$ [36], were prepared according to the literature procedures. Since only the room temperature crystal structure and magnetic moment of the cobalt complex have been reported before, we undertook its full magnetochemical characterization and a low temperature structure determination (Fig. 1). The crystal structure of $[Co(bpp)_2][BF_4]_2$ at 150 K is essentially identical to the previously published 290 K structure, with only some minor differences in bond angles being evident between the two temperatures (Fig. 1). Although crystallographic Co–N distances in this type of compound are not very sensitive the metal ion spin state, the metric parameters in the $[Co(bpp)_2]^{2+}$ cation are consistent with a high-spin complex of this type [33, 36], as predicted from the magnetic data. The cations pack in a variant of the well-known 'terpyridine embrace' lattice type, forming 2D layers through weak face-to-face π-π contacts between the pyrazolyl arms of the bpp ligands [30].
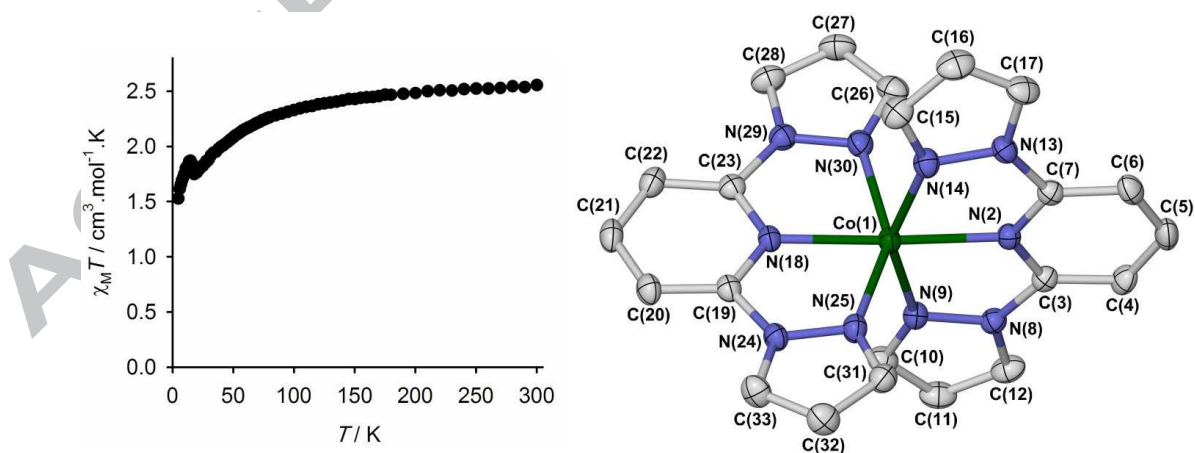

Fig. 1. Left: variable temperature magnetic susceptibility data from $[Co(bpp)_2][BF_4]_2$. Right: view of the $[Co(bpp)_2]^{2+}$ molecule in the low temperature crystal structure of $[Co(bpp)_2][BF_4]_2$.

A bulk sample of $[Co(bpp)_2][BF_4]_2$ exhibited $\chi_M T = 2.5$ cm^{3}mol^{-1}K at 300 K, a typical value for a high-spin cobalt(II) complex with this ligand type. The $\chi_M T$ value decreased increasingly rapidly as the temperature was lowered, reaching 1.5 cm^{3}mol^{-1}K at 5 K. This trend is characteristic for zero-field splitting of a high-spin cobalt centre, which can be particularly strong in six-coordinate cobalt(II) complexes [37]. Hence $[Co(bpp)_2][BF_4]_2$ is not spin-crossover active, and remains high-spin upon cooling. Consistent with that conclusion, $[Co(bpp)_2][BF_4]_2$ is EPR-silent at 120 K in the solid state and in MeCN solution. If it were spin-crossover active, the low-spin cobalt(II) fraction would lead to an observable, albeit potentially broadened, EPR peak on cooling [33, 38, 39].

In addition, the susceptibility curve exhibits an unusual discontinuity at 17 K, which might reflect a crystallographic phase change in the material [40, 41] (Fig. 1). In support of that suggestion, the isostructural copper(II) complex exhibits such a phase change at 41 K [42]. However, the very low temperature of this feature has prevented us from confirming that suggestion by diffraction methods. The feature could also be a function of weak intermolecular ferromagnetism in the material, although there are no directional obvious directional interactions between the cations in the crystal lattice to mediate such an interaction.

2.2 The $[Fe_xCo_{1-x}(bpp)_2][BF_4]_2$ solid solutions

Following our previous protocol [25, 27, 28], the iron and cobalt precursor compounds were co-crystallized from nitromethane solution, by slow diffusion of diethyl vapor. This yielded polycrystalline materials, which were lightly ground for characterization. Three compositions of solid $[Fe_xCo_{1-x}(bpp)_2][BF_4]_2$ were prepared, with $x = 0.95$ (**1a**), 0.85 (**1b**) and 0.77 (**1c**) by C, H, N and metal microanalyses. These compositions were chosen to match the materials from our earlier study of the $[Fe(bpp)_2]_y[Co(terpy)_2]_{1-y}[BF_4]_2$ system [$y = 0.97$ (**2a**), 0.85 (**2b**) and 0.76 (**2c**)]. Consistent with our previous studies on this system [25, 27], the metal stoichiometries of **1a**-**1c** closely matched the ratio of Fe:Co reagents in the crystallization vials. X-ray powder diffraction confirmed that **1a**-**1c** are phase-pure, and isostructural with the iron and cobalt precursor compounds (Fig. 2). The resolution of their powder patterns also implies they are highly crystalline.

Variable temperature magnetic susceptibility data show that the solid solution materials undergo thermal spin-crossover as expected (Fig. 3, Tables 1 and 2). Importantly, the $\chi_M T$ values at room temperature show that both the iron and cobalt centres in the material are predominantly high-spin. Below the transition temperature, however, $\chi_M T$ implies that the iron sites are low spin, but that the cobalt centres have remained high-spin (Table 2). Consistent with that, $\chi_M T$ for **1b** and **1c** clearly decreases below 100 K (Fig. 3), reflecting the stronger zero-field splitting of the high-spin $[Co(bpp)_2]^{2+}$ centres in the samples (Fig. 1). That also implies that the samples still contain high-spin cobalt centres below the spin-crossover $T_{\frac{1}{2}}$ temperatures. Therefore, the iron spin transition in **1a**-**1c** does not induce spin-crossover in the $[Co(bpp)_2]^{2+}$ dopand sites, in contrast to $[Co(terpy)_2]^{2+}$ in **2a**-**2c** [26, 27]. *X*-band EPR measurements again supported that conclusion since, unlike **2a**-**2c** [27], **1a**-**1c** are all EPR-silent at 120 K and above. That is consistent with their cobalt centres being fully high-spin in that temperature range [33, 38, 39].
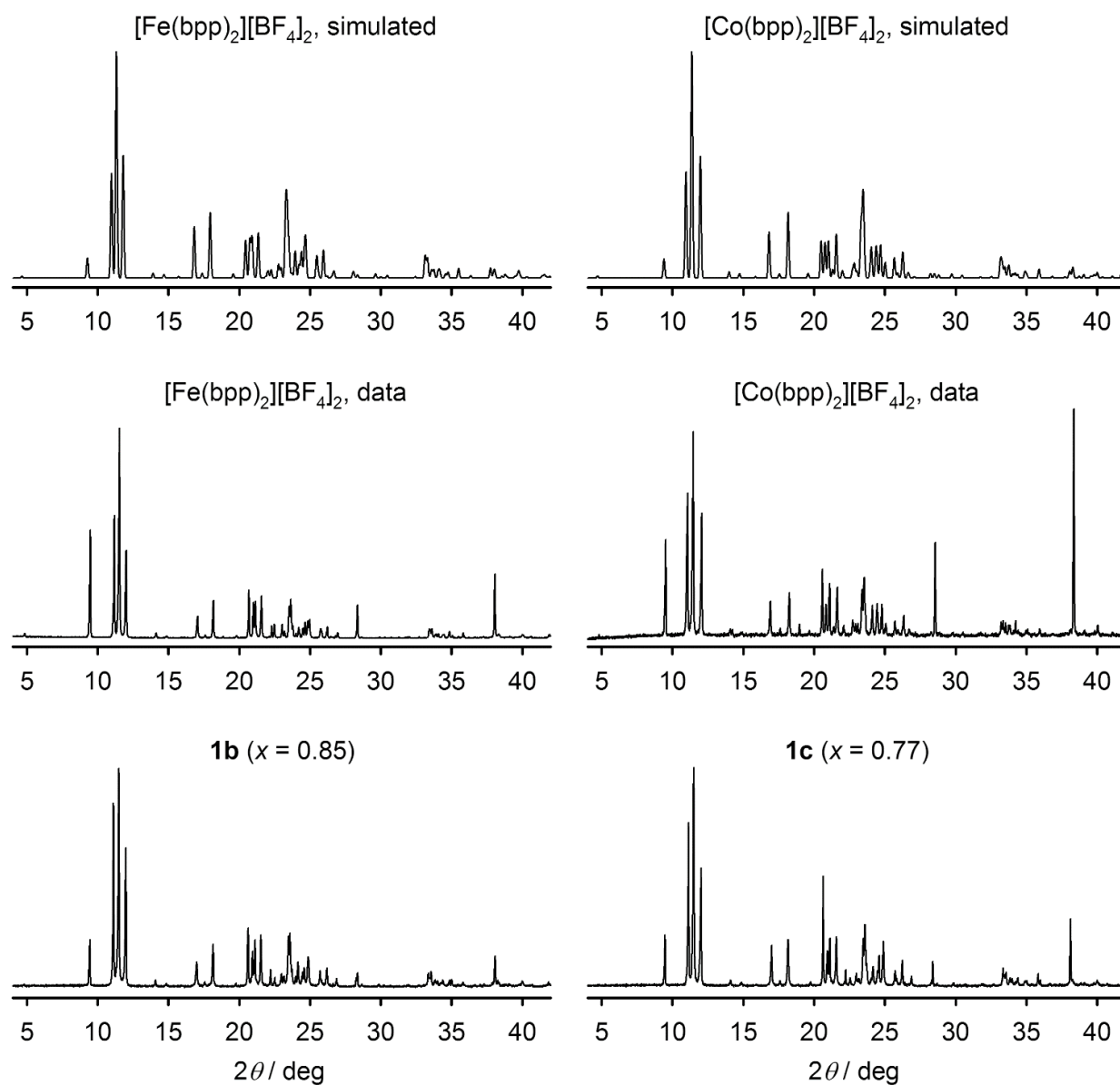
Fig. 2. Experimental X-ray powder diffraction data from compounds in this work, and simulations based on the room-temperature crystal structures of the precursor compounds. Data from **1a** are visually indistinguishable from those of **1b**. The greater-than-expected intensity of the peak near $2\theta = 38.5°$ in each pattern is a preferred orientation effect from the manually ground polycrystalline samples.
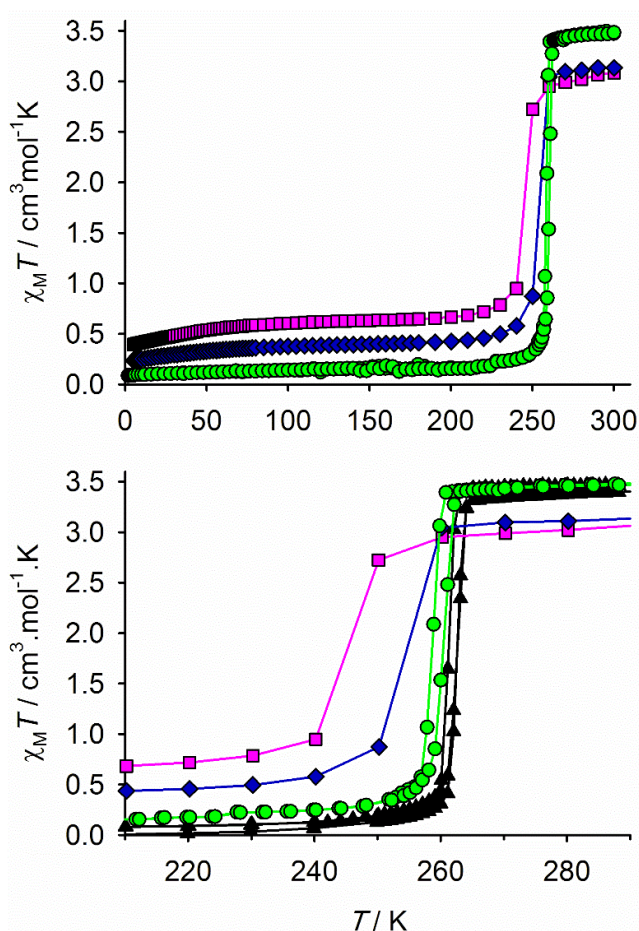
Fig. 3. Magnetic susceptibility data from **1a** (green circles), **1b** (blue diamonds) and **1c** (pink squares). Lines through the data are also shown, for clarity. Data for **1a** were measured in both cooling and warming mode, while the other two compounds are in warming mode only. Top: the complete temperature range of 5-300 K. Center: expansion of the spin-transitions, including pure [Fe(bpp)$_2$][BF$_4$]$_2$ (black triangles) for comparison [25].

Table 1 Observed values of $\chi_M T$ (cm^{3}mol^{-1}K) from high- and low-spin [Fe$_x$Co$_{1-x}$(1-bpp)$_2$][BF$_4$]$_2$ (**1a-1c**), compared with predicted values based on the analytical compositions of the samples. The reduced $\chi_M T$ values at 5 K are reduced by zero-field splitting of the remaining high-spin fraction of the sample.

		Calculated $\chi_M T$[a]		Observed $\chi_M T$		
	x	Low-spin iron + high-spin cobalt	High-spin iron + high-spin cobalt	5 K	100 K	300 K
1a	0.95	0.13	3.45	0.09	0.14	3.48
1b	0.85	0.38	3.35	0.24	0.37	3.13
1c	0.77	0.58	3.27	0.39	0.60	3.09

[a] The calculated values are based on the following $\chi_M T$ values for the pure components of the solid solutions; high-spin [Fe(1-bpp)$_2$][BF$_4$]$_2$, = 3.5; low-spin [Fe(1-bpp)$_2$][BF$_4$]$_2$, 0; high-spin [Co(1-bpp)$_2$][BF$_4$]$_2$, 2.5; low-spin [Co(1-bpp)$_2$][BF$_4$]$_2$, 0.4 cm^{3}mol^{-1}K.

Table 2 Spin-crossover parameters for [Fe$_x$Co$_{1-x}$(1-bpp)$_2$][BF$_4$]$_2$ (**1a-1c**) from magnetic susceptibility and calorimetry data. Data from pure [Fe(bpp)$_2$][BF$_4$]$_2$ are also given for comparison [25]. ΔH and ΔS are quoted per mole of iron in the solid solutions.

		Magnetic measurements		DSC			
	x	$T_{1/2}\downarrow$ / K	$T_{1/2}\uparrow$ / K	$T_{1/2}\uparrow$ / K	ΔH / kJmol^{-1}	ΔS / Jmol^{-1}K^{-1}	Γ / kJmol^{-1}
[Fe(bpp)$_2$][BF$_4$]$_2$	1.00	261.0	262.5	263.2	21.8(2)	82.9(8)	6.4(2)
1a	0.95	258.6	260.4	260.4	17.5(2)	67.1(8)	6.3(3)
1b	0.85	–	254.7	253.7	14.3(3)	57(1)	5.2(2)
1c	0.77	–	245.7	247.8	12.3(3)	50(1)	4.6(3)

   Differential scanning calorimetry (DSC) measurements on a warming temperature ramp corroborated the transition temperatures from the magnetic data (Table 2). The dependence of ΔH and ΔS of spin-crossover on the dopant concentration for **1a-1c** is similar to the nickel solid solutions [25], which is another indication that spin-crossover in **1a-1c** does not involve the cobalt centers. The additional contribution from a switching dopant should lead to higher values of ΔH and ΔS compared to a comparable lattice with an inert dopant [27], which is not observed in **1a-1c**. $T_{1/2}$ decreases more rapidly with increasing dopant concentration (x) in **1a-1c** than in the analogous nickel-doped materials, [Fe$_z$Ni$_{1-z}$(1-bpp)$_2$][BF$_4$]$_2$ [25] (Fig. 4). That reflects the larger ionic radius of high-spin cobalt(II) (89 pm) compared to nickel(II) (83 pm), meaning the cobalt dopant in [Fe$_x$Co$_{1-x}$(1-bpp)$_2$]$^{2+}$ stabilizes the larger volume of the high-spin host lattice [43]. The spin-transition cooperativity, as expressed by the mean field interaction energy Γ (equation 1) [44], also decreases with x since propagation of the transition is impaired by the inert dopant metal lattice sites (Table 2) [43]:

$$\ln\left[\frac{1-n_{HS}}{n_{HS}}\right] = \frac{\Delta H(x) + x(1-2n_{HS})\Gamma}{RT} - \frac{\Delta S(x)}{R} \tag{1}$$

where n_{HS} is the high-spin fraction at temperature T and x is the fractional iron concentration, as above. The reduction in Γ for a given dopant concentration is also apparently greater for **1a-1c** than for the nickel(II) series [25], although further studies would be required to confirm that observation [43, 44].
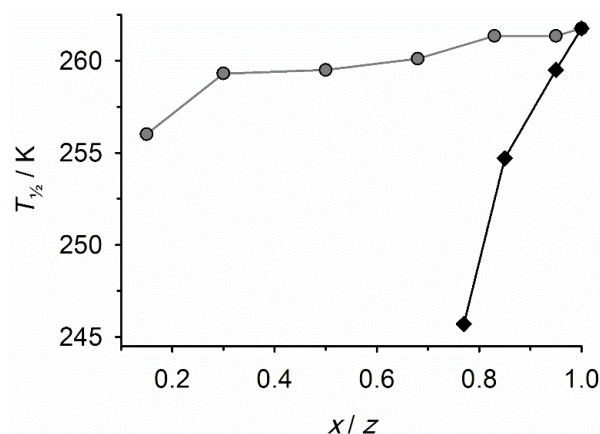
Fig. 4. Variation of $T_{1/2}$ with the metal dilution factor in [Fe$_x$Co$_{1-x}$(1-bpp)$_2$][BF$_4$]$_2$ (**1a-1c**; black diamonds) and the corresponding [Fe$_z$Ni$_{1-z}$(1-bpp)$_2$][BF$_4$]$_2$ series (grey circles) [25].

2.3 LIESST effect

Salts of $[Fe(bpp)_2]^{2+}$ derivatives are well known to exhibit photomagnetic effects at low temperatures [26, 45, 46]. The low-spin→high-spin (LS→HS) photoconversion of **1a-1c** was investigated on powder samples using a SQUID magnetometer coupled to a CW optical source. Thin layers of the samples were irradiated at the following wavelengths: 405, 510, 640, 830 and 980 nm. In each case, the most efficient wavelength to induce the LIESST effect was found to be 510 nm, leading to a strong increase of the magnetic signal at 10 K. No reverse-LIESST was observed upon irradiation at the highest wavelengths (830 and 980 nm), however. Using our standardized T(LIESST) procedure [47, 48] we monitored the direct magnetic response of compounds **1a-1c** upon irradiation and after it was switched off. The T(LIESST) curves were then recorded for each compound (Fig. 5) to determine the thermal relaxation of the photoinduced HS state.

Fig. 5. Temperature dependence of $\chi_M T$ for **1a** (a), **1b** (b) and **1c** (c): thermal behavior of $\chi_M T$ before irradiation (■), during irradiation (△) at 510 nm at 10 K, and the T(LIESST) measurement in the warming mode when the laser was switched off (■). Inset: first derivative of the $\chi_M T$ *vs.* T curve, recorded in the dark after irradiation, whose minimum gives T(LIESST).

A drastic increase in the magnetic signal under green light irradiation was observed for all the compounds at 10 K, with an almost quantitative photoconversi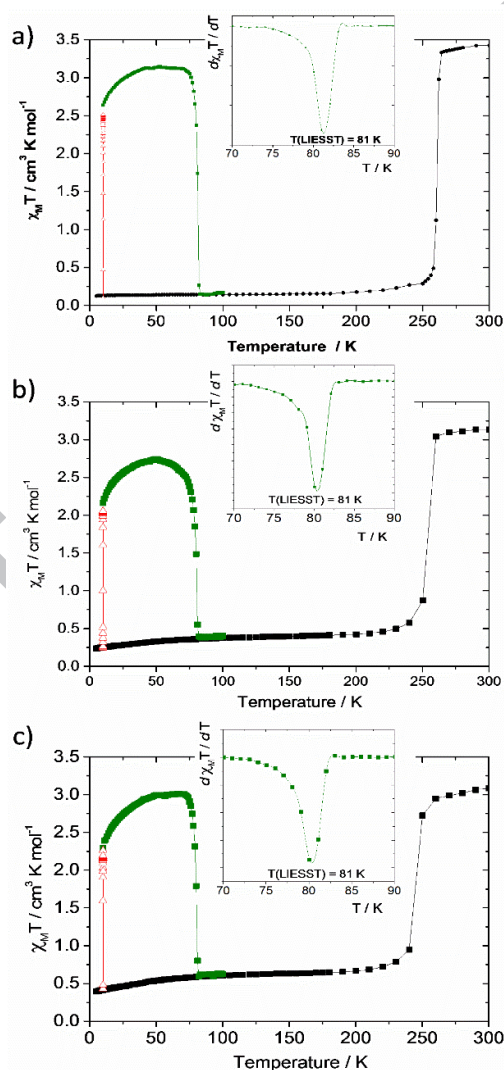on efficiency. Following the irradiation procedure, an increase in $\chi_M T$ occurs upon heating from 10 K in the dark, reflecting zero-field splitting of the HS iron(II) centers [49]. Above 75 K, the light-induced metastable HS state rapidly relaxes, and $\chi_M T$ reaches the baseline above 80 K. The fact that the T(LIESST) curves do not extend below their original baseline shows the photo-conversion process only involves the iron(II) fraction of the samples. The T(LIESST) values can be extracted from the first derivative of the $\chi_M T$ vs. T curves (Fig. 5, inset). For the three compounds T(LIESST) = 80 K. First of all, the [T(LIESST), $T_{1/2}$] values of **1a-1c** fall close to the T_0 = 150 K line of the T(LIESST) vs $T_{1/2}$ database [48], in common with most other [Fe(bpp)$_2$]$^{2+}$ derivatives that have been measured by this procedure [45, 46]. Secondly, according to this database, a decrease of $T_{1/2}$ should induce an increase of T(LIESST). In **1a-1c**, the constant value of T(LIESST) upon metal dilution, despite the decrease in $T_{1/2}$, apparently contradicts this prediction but is consistent with previous observations on solid solutions [50]. These observations emphasize the molecular character of the T(LIESST) curve compared to the macroscopic behavior of the thermal SCO.

The relaxation dynamics of the photo-induced HS fraction, γ_{HS}, were investigated for all three complexes in the 66-80K temperature range where the HS→LS relaxation is thermally activated. The value of γ_{HS} was deduced from the equation $[(\chi_M T)_{hv} - (\chi_M T)_{LS}]/[(\chi_M T)_{HS} - (\chi_M T)_{LS}]$, in which $(\chi_M T)_{hv}$ is the magnetic value reached after irradiation, $(\chi_M T)_{LS}$ is the magnetic value of the initial LS state, and $(\chi_M T)_{HS}$ is the magnetic value recorded at room temperature for a fully HS state. The relaxation kinetics of **1a-1c** are presented in Fig. 6. The relaxation behavior of all the compounds deviates strongly from a single exponential. The sigmoidal shape of the relaxation curves of **1a** can be described by the self-accelerated process described by Hauser which reflects the change in the energy barrier as a function of γ_{HS} in cooperative SCO materials [43] (eq (1) and (2), with $\alpha = E_a*/k_B T$ and $k_{HL} = k_\infty \exp(-E_a/k_B T)$).

$$\frac{\partial \gamma_{HS}}{\partial t} = -k^*_{HL}\gamma_{HS} \tag{1}$$

$$k^*_{HL}(T, \gamma_{HS}) = k_{HL}(T)\exp[\alpha(T)(1 - \gamma_{HS})] \tag{2}$$

Simulation of the relaxation kinetics of **1a** lead to the following thermodynamic parameters, which are similar to those of other comparable solid solutions of [Fe(bpp)$_2$][BF$_4$]$_2$ [26]: E_a = 1210 cm^{-1}, k_∞ = 9.2 10^5 s^{-1} and E_a* = 245 cm^{-1}. However, the relaxation curves for **1b** and **1c** clearly exhibit multistep character. At least two inflexion points can be seen as reflecting the presence of two self-accelerated relaxation processes, both of them being probably stretched. These can't be attributed to separate relaxation of the iron and cobalt centers [26], since the cobalt ions are not involved in the LIESST process as above. Alternative hypotheses to explain this behavior include the following. First, despite the phase homogeneity of the powder samples (Fig. 2), microscopic segregation of the iron and cobalt fractions of the sample may occur. Although no such phase separation has been detected before in this system [25-28], a detailed study well below the microscopic scale would be required to confirm or discard that hypothesis. Second, crystal quality affects the number of coherent domains and nucleation sites in a solid material, which can lead to multistep HS→LS relaxations [51]. Finally, some

unexpected symmetry breaking could occur during the relaxation due to elastic frustration caused by metal dilution [46]. While deviations from idealized relaxation behavior can also reflect to molecular conformation or disorder during the LIESST excitation [52], such effects have not been observed before in the [Fe(bpp)]$_2$[BF$_4$]$_2$ system [45].
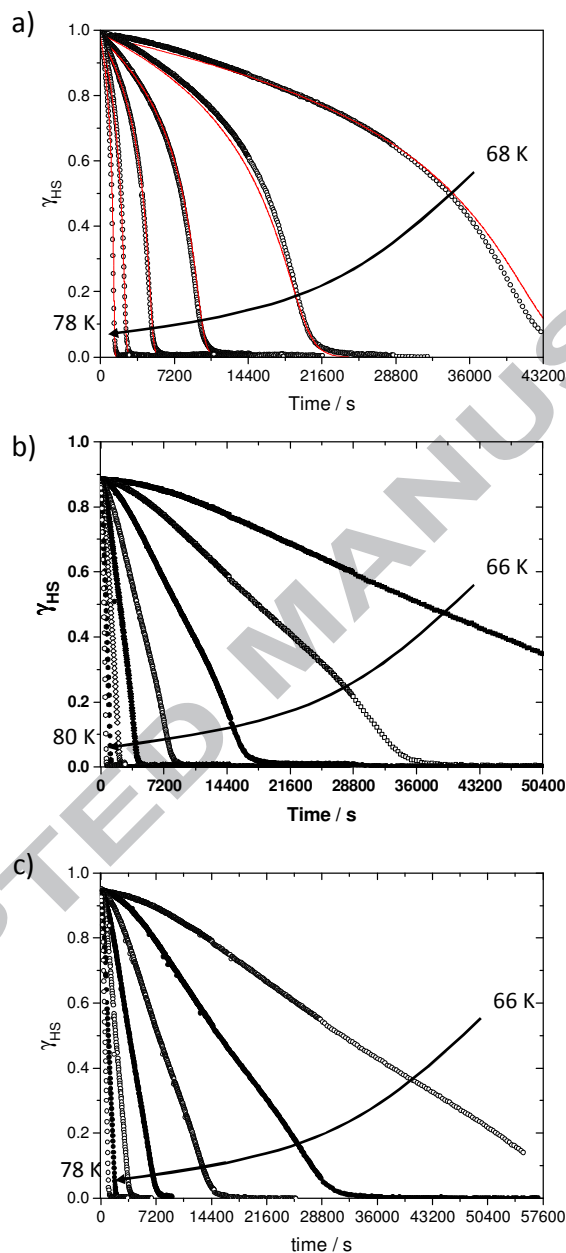

Fig. 6. HS→LS relaxation kinetics for **1a** (a), **1b** (b) and **1c** (c) at temperatures between 66 K and 80 K. The red lines in (a) show the simulations discussed in the text.

3. Conclusions

In contrast to the $[Fe(bpp)_2]_y[Co(terpy)_2]_{1-y}[BF_4]_2$ system (**2a**-**2c**) [26, 27], thermal and light-induced spin-crossover in $[Fe_xCo_{1-x}(bpp)_2][BF_4]_2$ (**1a**-**1c**) does not involve allosteric switching of the iron and cobalt sites. Rather, the $[Co(bpp)_2]^{2+}$ centers in **1a**-**1c** remain high-spin at all temperatures, during both thermal-crossover and LESST excitation and relaxation processes. That reflects the spin-state properties of the different dopant compounds: while $[Co(terpy)_2][BF_4]_2$ undergoes an extremely gradual spin-crossover equilibrium between *ca.* 100-400 K as a neat solid [39], $[Co(bpp)_2][BF_4]_2$ is a purely high-spin material. Hence, a greater increase in lattice pressure should be required to induce a high→low spin-state change in a $[Co(bpp)_2]^{2+}$ dopant, than in $[Co(terpy)_2]^{2+}$. Evidently the 2 % lattice contraction during the spin-transition in the $[Fe(bpp)_2][BF_4]_2$ host lattice [32] is not sufficient to induce spin-crossover in the more challenging dopant $[Co(bpp)_2]^{2+}$.

The LIESST behavior of the two series of compounds also differs in other ways. While the *T*(LIESST) decreases slightly as *y* increases in **2a**-**2c** [26], it remains constant in the $[Fe_xCo_{1-x}(bpp)_2][BF_4]_2$ compounds. The latter behavior is more common in LIESST studies of metal-diluted materials [50]. The relaxation kinetics also strongly differ from one system to the other. In **2a**-**2c**, the relaxation is always self-accelerated and involve concomitantly the iron(II) and the cobalt(II) ions [26]. In contrast, in **1a**-**1c** the HS→LS relaxation has a multistep character whose origin is currently uncertain, but should not involve the cobalt(II) ion which always remains high-spin where this can be measured.

Current work aims to clarify the microscopic composition of our solid solutions, to shed insight into the observed dependence of their LIESST behavior on the type of dopant present. We also seek to identify new host lattices that undergo a larger contraction during spin-crossover, that may induce new switching processes in apparently inert dopant molecules.

4. Experimental Section

4.1 Instrumentation

CHN microanalyses were performed by the University of Leeds School of Chemistry microanalytical service, while metal analyses were carried out by the microanalytical service at the University of Manchester. Powder diffraction data were obtained with a Bruker D8 diffractometer using Cu radiation (λ = 1.5418 Å). DSC measurements employed a TA Instruments DSC 2010 scanning calorimeter, with a temperature ramp of 5 Kmin^{-1}. *X*-band EPR spectra were run using a Bruker EMX spectrometer fitted with an ER4119HS resonator and ER4131VT cryostat. Variable temperature magnetic susceptibility measurements were obtained using a Quantum Design SQUID magnetometer, with an applied field of 5 kG and a temperature ramp of 2 Kmin^{-1}. Midpoint temperatures for the spin-transitions ($T_{1/2}$) were calculated based on the Fe:Co compositions derived by microanalysis. Diamagnetic corrections for the sample (from Pascal's constants [53]) and the sample holder were applied to the data. The mean field cooperativity fits to the susceptibility data (equation 1) were performed with *SIGMAPLOT* [54], using fixed ΔH and ΔS values from the DSC measurements.

Photomagnetic measurements were performed using a set of photodiodes coupled via an optical fibre to the cavity of a MPMS-55 Quantum Design SQUID magnetometer operating at 20,000 G. The powder sample was prepared in a thin layer (~0.1 mg on around 100 µm thickness) to promote full

penetration of the irradiated light. The sample mass was obtained by comparison with the thermal spin transition curve measured on a larger, accurately weighed polycrystalline sample. The sample was first slow cooled to 10 K, ensuring that potential trapping of HS species at low temperatures did not occur. Irradiation was carried out at 405, 510, 650, and 830 nm and the power of the sample surface was adjusted to 5 mW cm^{-2} (calibrated outside the SQUID magnetometer). Irradiation at 510 nm was found to be most efficient in this system. Once photo-saturation was reached, irradiation was ceased and the temperature increased at a rate of 0.3 K min^{-1} to ~100 K and the magnetization measured every 1 K to determine the T(LIESST) value given by the minimum of the $\delta\chi_M T/\delta T$ *vs T* curve for the relaxation [46-47]. The T(LIESST) value describes the limiting temperature above which the light-induced magnetic high-spin information is erased in a SQUID cavity. In the absence of irradiation, the magnetisation was also measured over the temperature range 10–290 K to follow the thermal spin transition and to obtain a low temperature baseline. Kinetic studies of LIESST relaxation were performed by irradiating the sample at 10 K until photo-saturation, then, under constant irradiation the sample was warmed to a desired temperature around the T(LIESST) region. When the desired temperature is stable, irradiation is stopped and the decay of the magnetization signal is followed for several hours, or until complete relaxation back to the low-spin baseline, after 10 seconds of thermalization.

4.2 Synthesis

The precursor compounds [Fe(bpp)$_2$][BF$_4$]$_2$ [32] and [Co(bpp)$_2$][BF$_4$]$_2$ [36] were prepared as previously described. The solid solutions **1a-1c** were prepared by co-crystallising these two compounds in Fe:Co molar ratios of 0.95:0.05 (**1a**), 0.85:0.15 (**1b**) and 0.75:0.25 (**1c**) from nitromethane/diethyl ether mixtures. Elemental analysis data for the compounds in this work are given in Table 3.

Table 3 Measured and (calculated) elemental microanalyses for the compounds in this work.

	z	C	H	N	Fe	Co
[Fe(bpp)$_2$][BF$_4$]$_2$	1.00	40.3 (40.5)	2.75 (2.78)	21.5 (21.5)	8.3 (8.6)	–
[Co(bpp)$_2$][BF$_4$]$_2$	0	40.4 (40.3)	2.65 (2.77)	21.4 (21.4)	–	8.8 (9.0)
[Fe$_{0.95}$Co$_{0.05}$(bpp)$_2$][BF$_4$]$_2$ (**1a**)	0.95	40.5 (40.5)	2.75 (2.78)	21.5 (21.5)	7.9 (8.1)	0.3 (0.5)
[Fe$_{0.85}$Co$_{0.15}$(bpp)$_2$][BF$_4$]$_2$ (**1b**)	0.85	40.6 (40.5)	2.65 (2.78)	21.5 (21.5)	7.1 (7.3)	1.3 (1.4)
[Fe$_{0.77}$Co$_{0.23}$(bpp)$_2$][BF$_4$]$_2$ (**1c**)	0.77	40.3 (40.5)	2.75 (2.78)	21.5 (21.5)	6.7 (6.6)	2.2 (2.1)

4.3 Crystal structure determination.

Single crystals of [Co(bpp)$_2$][BF$_4$]$_2$ were grown by slow diffusion of diethyl ether vapor into a nitromethane solution of the complex. Diffraction data were measured using a Bruker X8 Apex diffractometer, with graphite-monochromated Mo-K_α radiation (λ = 0.71073 Å) generated by a

rotating anode. The diffractometer is fitted with an Oxford Cryosystems low temperature device. Experimental details of the structure determination are given in Table 4. The structures was solved by direct methods *(SHELXS97* [55]), and developed by full least-squares refinement on F^2 *(SHELXL97* [55]). Crystallographic figures were prepared using *XSEED* [56].

No disorder was included in the model, and no restraints were applied to the refinement. All non-H atoms were refined anisotropically, while H atoms were placed in calculated positions and refined using a riding model

Table 4 Experimental details for the low-temperature crystal structure of [Co(bpp)$_2$][BF$_4$]$_2$

formula	$C_{22}H_{18}B_2CoF_8N_{10}$	D_{calcd} / Mgm^{-3}	1.609
M_r	655.01	μ / mm^{-1}	0.724
crystal class	monoclinic	measured reflections	21879
space group	$P2_1$	unique reflections	5444
a / Å	8.5019(7)	observed reflections	5185
b / Å	8.5060(6)	R_{int}	0.052
c / Å	18.8550(14)	R_1 [$Fo>4\sigma(Fo)$][a]	0.027
β / °	97.563(3)	wR_2 [all data][b]	0.071
V / Å^3	1351.68(18)	GoF	1.054
Z	2	Flack parameter	0.012(9)
T / K	150(2)		

[a] $R = \Sigma[|F_o| - |F_c|] / \Sigma|F_o|$. [b] $wR = [\Sigma w(F_o^2 - F_c^2) / \Sigma w F_o^4]^{1/2}$.

Acknowledgments

Appendix A. Supplementary data

Metric parameters from the crystal structure; DSC data; and other figures relevant to the analysis of the magnetic and photomagnetic data are given in supplementary material. CCDC-1517546 contains the supplementary crystallographic data for this paper. These data can be obtained free of charge via http://www.ccdc.cam.ac.uk/conts/retrieving.html, or from the Cambridge Crystallographic Data Centre, 12 Union Road, Cambridge CB2 1EZ, UK; fax: (+44) 1223-336-033; or e-mail: deposit@ccdc.cam.ac.uk. Supplementary data associated with this article can be found, in the online version, at http://dx.doi.org/10.1016/j.poly.####

References

[1] P. Gütlich, H. A. Goodwin, (eds.), Spin Crossover in Transition Metal Compounds I-III. Topics in Current Chemistry vols. 233-235; Springer, Berlin, Germany (2004).

[2] M. A. Halcrow (ed), Spin-crossover materials – properties and applications; John Wiley & Sons, Chichester, UK (2013) p. 568.

[3] P. Gütlich, Eur. J. Inorg. Chem. (2013), 581–591.

[4] A. H. Ewald, R. L. Martin, I. G. Ross, A. H. White, Proc. Royal Soc. London. Ser. A 280 (1964), 235.

[5] H. J. Shepherd, G. Molnár, W. Nicolazzi, L. Salmon, A. Bousseksou, Eur. J. Inorg. Chem. (2013) 653–661.

[6] J. Linares, E. Codjovi, Y. Garcia, Sensors 12 (2012) 4479.

[7] O. S. Wenger, Chem. Rev. 113 (2013) 3686.

[8] A. B. Gaspar, M. Seredyuk, Coord. Chem. Rev. 268 (2014) 41.

[9] M. D. Manrique-Juárez, S. Rat, L. Salmon, G. Molnár, C. M. Quintero, L. Nicu, H. J. Shepherd, A. Bousseksou, Coord. Chem. Rev. 308 (2016) 395.

[10] A. B. Gaspar, V. Ksenofontov, M. Seredyuk, P. Gütlich, Coord. Chem. Rev. 249 (2005) 2661.

[11] L. Salmon, G. Molnár, D. Zitouni, C. Quintero, C. Bergaud, J.-C.Micheau, A. Bousseksou, J. Mater. Chem. 20 (2010) 5499.

[12] Y. Garcia, F. Robert, A. D. Naik, G. Zhou, B. Tinant, K. Robeyns, S. Michotte, L. Piraux, J. Am. Chem. Soc. 133 (2011) 15850.

[13] R. González-Prieto, B. Fleury, F. Schramm, G. Zoppellaro, R. Chandrasekar, O. Fuhr, S. Lebedkin, M. Kappes, M. Ruben, Dalton Trans. 40 (2011) 7564.

[14] C.-F. Wang, R.-F. Li, X.-Y. Chen, R.-J. Wei, L.-S. Zheng, J. Tao, Angew. Chem. Int. Ed. 54 (2015) 1574.

[15] J. M. Herrera, S. Titos-Padilla, S. J. A. Pope, I. Berlanga, F. Zamora, J. J. Delgado, K. V. Kamenev, X. Wang, A. Prescimone, E. K. Brechin, E. Colacio, J. Mater. Chem. C 3 (2015) 7819.

[16] K. Takahashi, H.-B. Cui, Y. Okano, H. Kobayashi, H. Mori, H. Tajima, Y. Einaga, O. Sato, J. Am. Chem. Soc. 130 (2008) 6688.

[17] M. Nihei, N. Takahashi, H. Nishikawa, H. Oshio, Dalton Trans. 40 (2011) 2154.

[18] W. Xue, B.-Y. Wang, J. Zhu, W.-X. Zhang, Y.-B. Zhang, X.-X. Zhao, X.-M. Chen, Chem. Commun. 47 (2011) 10233.

[19] A. Rotaru, I. A. Gural'skiy, G. Molnár, L.Salmon, P. Demont, A. Bousseksou, Chem. Commun. 48 (2012) 4163.

[20] H. Phan, S. M. Benjamin, E. Steven, J. S. Brooks, M. Shatruk, Angew. Chem. Int. Ed. 54 (2015) 823.

[21] M. Nakano, G. Matsubayashi, T. Matsuo, Phys. Rev. B 66 (2002) 212412/1.

[22] A. Bousseksou, G. Molnár, P. Demont, J. Menegotto, J. Mater. Chem. 13 (2003) 2069.

[23] S. Bonhommeau, T. Guillon, M. L. M. Daku, P. Demont, J. S. Costa, J.-F. Létard, G. Molnár, A. Bousseksou, Angew. Chem. Int. Ed. 45 (2006) 1625.

[24] X. Zhang, S. Mu, G. Chastanet, N. Daro, T. Palamarciuc, P. Rosa, J.-F. Létard, J. Liu, G. E. Sterbinsky, D. A. Arena, C. Etrillard, B. Kundys, B. Doudin, P. A. Dowben, J. Phys. Chem. C 119 (2015) 16293.

[25] C. A. Tovee, C. A. Kilner, J. A. Thomas, M. A. Halcrow, CrystEngComm 11 (2009) 2069.

[26] G. Chastanet, C. A. Tovee, G. Hyett, M. A. Halcrow, J.-F. Létard, Dalton Trans. 41 (2012) 4896.

[27] M. A. Halcrow, Chem. Commun. 46 (2010) 4761.

[28] R. Docherty, F. Tuna, C. A. Kilner, E. J. L. McInnes, M. A. Halcrow, Chem. Commun. 48 (2012) 4055.

[29] L. J. Kershaw Cook, M. A. Halcrow, Polyhedron 87 (2015) 91.

[30] I. Dance, M. Scudder, CrystEngComm 11 (2009) 2233.

[31] R. Pritchard, C. A. Kilner, M. A. Halcrow, Chem. Commun. (2007) 577.

[32] J. M. Holland, J. A. McAllister, C. A. Kilner, M. Thornton-Pett, A. J. Bridgeman, M. A. Halcrow, J. Chem. Soc. Dalton Trans. (2002) 548.

[33] I. Krivokapic, M. Zerara, M. L. Daku, A. Vargas, C. Enachescu, C. Ambrus, P. Tregenna-Piggott, N. Amstutz, E. Krausz, A. Hauser, Coord. Chem. Rev. 251 (2007) 364.

[34] J.-F. Létard, J. Mater. Chem. 16 (2006) 2550.

[35] D. L. Jameson, K. A. Goldsby, J. Org. Chem. 55 (1990) 4992.

[36] J. M. Holland, C. A. Kilner, M. Thornton-Pett, M. A. Halcrow, Polyhedron 20 (2001) 2829,

[37] R. Boča, Coord. Chem. Rev. 248 (2004) 757.

[38] S. Kremer, W. Henke, D. Reinen, Inorg. Chem. 21 (1982) 3013.

[39] C. A. Kilner, M. A. Halcrow, Dalton Trans. 39 (2010) 9008.

[40] Y. Umezono, W. Fujita, K. Awaga, J. Am. Chem. Soc. 128 (2006) 1084.

[41] G. Juhász, R. Matsuda, S. Kanegawa, K. Inoue, O. Sato, K. Yoshizawa, J. Am. Chem. Soc. 131 (2009) 4560.

[42] M. A. Leech, N. K. Solanki, M. A. Halcrow, J. A. K. Howard, S. A. Dahaoui, Chem. Commun. (1999) 2245.

[43] A. Hauser, J. Jeftić, H. Romstedt, R. Hinek, H. Spiering, Coord. Chem. Rev. 190–192 (1999) 471.

[44] a) J.-P. Martin, J. Zarembowitch, A. Dworkin, J. G. Haasnoot, E. Codjovi, Inorg. Chem. 33 (1994) 2617;

b) J.-P. Martin, J. Zarembowitch, A. Bousseksou, A. Dworkin, J. G. Haasnoot, F. Varret, Inorg. Chem. 33 (1994) 6325.

[45] a) S. Marcen, L. Lecren, L. Capes, H. A. Goodwin, J-F. Létard, Chem. Phys. Lett. 358 (2002) 87;

b) C. Carbonera, J. S. Costa, V. A. Money, J. Elhaïk, J. A. K. Howard, M. A. Halcrow, J.-F. Létard, Dalton Trans. (2006) 3058;

c) C. Carbonera, C. A. Kilner, J.-F. Létard, M. A. Halcrow, Dalton Trans. (2007) 1284;

d) V. A. Money, C. Carbonera, J. Elhaïk, M. A. Halcrow, J. A. K. Howard, J.-F. Létard, Chem. Eur. J. 13 (2007) 5503;

e) M. Nihei, H. Tahira, N. Takahashi, Y. Otake, Y. Yamamura, K. Saito, H. Oshio, J. Am. Chem. Soc. 132 (2010) 3553;

f) I. Šalitroš, L. Pogány, M. Ruben, R. Boča, W. Linert, Dalton Trans. 43 (2014) 16584;

g) L. J. Kershaw Cook, F. L. Thorp-Greenwood, T. P. Comyn, O. Cespedes, G. Chastanet, M. A. Halcrow, Inorg. Chem. 54 (2015) 6319.

[46] L. J. Kershaw Cook, H. J. Shepherd, T. P. Comyn, C. Baldé, O. Cespedes, G. Chastanet, M. A. Halcrow, Chem. Eur. J. 21 (2015) 4805.

[47] J.-F. Létard , P. Guionneau, L. Rabardel, J. A. K. Howard, A. Goeta, D. Chasseau, O. Kahn, Inorg. Chem. 37 (1998) 4432.

[48] a) J.-F. Létard, P. Guionneau, O. Nguyen, J. S. Costa, S. Marcen, G. Chastanet, M. Marchivie, L. Capes, Chem. Eur. J. 11 (2005) 4582;

b) J.-F. Létard, G. Chastanet, P. Guionneau, C. Desplanches in Spin-crossover materials – properties and applications, M. A. Halcrow (ed.), John Wiley & Sons, Chichester, UK (2013) ch. 19, pp. 475–506.

[49] O. Kahn, Molecular Magnetism, VCH, Weinheim, Germany (1993), p.380.

[50] a) C. Baldé, C. Desplanches, P. Gütlich, E. Freysz, J.-F. Létard, Inorg. Chim. Acta. 361 (2008) 3529;

b) C. Baldé, C. Desplanches, A. Wattiaux, P. Guionneau, P. Gütlich, J.-F. Létard, Dalton Trans. (2008) 2702;

c) C. Baldé, C. Desplanches, O. Nguyen, J.-F. Létard, J. Phys. Conf. Ser. 148 (2009) 012026/1-012026/9;

d) G. Lebedev, S. Pillet, C. Baldé, P. Guionneau, C. Desplanches, J.-F. Létard, IOP Conf. Ser.: Mater. Sci. Eng. 5 (2009) 012025 ;

e) C. Baldé, C. Desplanches, M. Grunert, Y. Wei, P. Gütlich, J.-F. Létard, Eur. J. Inorg. Chem. (2008) 5382.

f) I. Krivokapic, P. Chakraborty, C. Enachescu, R. Bronisz, A. Hauser, Inorg. Chem. 50 (2011) 1856;

g) P. Chakraborty, C. Enachescu, C. Walder, R. Bronisz, A. Hauser, Inorg. Chem. 51 (2012) 9714;

h) N. Paradis, G. Chastanet, J.-F. Létard, Eur. J. Inorg. Chem. (2012) 3618;

i) N. Paradis, G. Chastanet, F. Varret, J.-F. Létard, Eur. J. Inorg. Chem. (2013) 968;

j) C. Baldé, C. Desplanches, F. Le Gac, P. Guionneau, J.-F. Létard, Dalton Trans. 43 (2014) 7820;

k) N. Paradis, G. Chastanet, T. Palamarciuc, P. Rosa, F. Varret, K. Boukheddaden, J.-F. Létard, J. Phys. Chem. C 119 (2015) 20039.

[51] a) I. Krivokapic, C. Enachescu, R. Bronisz, A. Hauser, Inorg. Chim. Acta 361 (2008) 3616;

b) P. Chakraborty, C. Enacheschu, A. Hauser, Eur. J. Inorg. Chem. (2013) 770.

[52] a) T. Buchen, P. Gütlich, Chem. Phys. Lett. 220 (1994) 262;

b) A. F Stassen, O. Roubeau, I. F. Gramage, J. Linarès, F. Varret, I. Mutikainen, U. Turpeinen, J. G. Haasnoot, J. Reedijk, Polyhedron 20 (2001) 1699;

b) G. A. Craig, J. S. Costa, S. J. Teat, O. Roubeau, D. S. Yufit, J. A. K. Howard, G. Aromí, Inorg. Chem. 52 (2013) 7203.

[53] C. J. O'Connor, Prog. Inorg. Chem. 29 (1982) 203.

[54] SIGMAPLOT, v. 8.02, SPSS Scientific Inc., Chicago IL (2002).

[55] G. M. Sheldrick, Acta Cryst. Sect. A 64 (2008) 112.

[56] L. J. Barbour, J. Supramol. Chem. 1 (2001) 189.